Electronic Supplementary Material (ESI) for ChemComm.

Supporting Information

Structure-Simplified and Highly Efficient Deep Blue Organic Light-Emitting Diodes with Reduced Efficiency Roll-Off at Extremely High Luminance

Xiang-Long Li, Ming Liu, Yunchuan Li, Xinyi Cai, Dongcheng Chen, Kunkun Liu, Yong Cao and Shi-Jian Su*

State Key Laboratory of Luminescent Materials and Devices, Institute of Polymer Optoelectronic Materials and Devices, South China University of Technology, Guangzhou, 510640, P. R. China

E-mail: mssjsu@scut.edu.cn

1. Experimental

General Methods. The NMR data were collected on a Bruker AVANCE Digital 600 MHz NMR workstation at room temperature. Matrix-assisted laser desorption ionization time-of-flight (MALDI-TOF) mass spectra were recorded on a Bruker Autoflex III Smartbean. Mass spectrometry (MS) data were obtained on a Waters TQD. Differential scanning calorimetry (DSC) measurements were performed on a Netzsch DSC 209 under a N_2 flow at a heating and cooling rate of 10 °C min^{-1}. Thermogravimetric analyses (TGA) were performed on a Netzsch TG 209 under a N_2 flow at a heating rate of 10 °C min^{-1}. Ultraviolet-visible (UV-vis) absorption spectra were recorded on a SHIMADZU UV-vis spectrophotometer, UV-2600. Photoluminescence (PL) spectra were measured by using a Jobin-Yvon spectrofluorometer. Cyclic voltammetry (CV) was performed on a CHI600D electrochemical workstation with a Pt working electrode and a Pt wire counter electrode at a scanning rate of 100 mV s^{-1} against a Ag/Ag^+ (0.1 M of $AgNO_3$ in acetonitrile) reference electrode with a nitrogen-saturated anhydrous acetonitrile and dichloromethane (DCM) solution of 0.1 mol L^{-1} tetrabutylammoniumhexafluorophosphate. PL quantum yields (PLQY) of the solutions and films were measured by using an integrating sphere on a HAMAMATSU absolute PL quantum yield spectrometer C11347. Transient PL was measured by a HAMAMATSU compact Fluorescence Lifetime Spectrometer C11367. All reagents for synthesis were obtained from Alfa Aesar or Sigma-Aldrich and were used without further purification.

Materials*.* Methods of the synthesis of **1-1**, and **2-1** were described in our earlier literature.[3]

NI-1-PhBr: **1-1** (2.20 g, 9.4 mmol) was combined with 4'-bromo-[1,1'-biphenyl]-4-carbaldehyde (2.00 g, 7.7 mmol) and 100 mL of 2-ethoxyethanol. The mixture was heated to 140 ºC for 24 h. After being cooled to room temperature, the reaction mixture was poured into 300 mL of water and extracted with DCM. The organic phases were combined and dried over $MgSO_4$. After the solvent was removed, the crude product was purified by column chromatography on silica gel to yield a white solid product (2.23 g, yield 61%).

NI-2-PhBr: NI-2-PhBr was synthesized according to the procedure as described above for the synthesis of *NI-1-PhBr*, giving a white solid in 69% yield.

NI-1-DPhTPA (N,N-diphenyl-4'''-(3-phenyl-3H-naphtho[1,2-*d*]imidazol-2-yl)-[1,1':4',1'':4'',1'''-quaterphenyl]-4-amine*):* Toluene (60 mL), ethanol (20 mL), and 2 M aqueous Na_2CO_3 (15 mL) were added to a mixture of *NI-1-PhBr* (1.42 g, 3 mmol), N,N-diphenyl-4'-(4,4,5,5-tetramethyl-1,3,2-dioxaborolan-2-yl)-[1,1'-biphenyl]-4-amine (1.38 g, 3.1 mmol), and $Pd(PPh_3)_4$ (100 mg, 3 mol%). The suspension was stirred at 90 ºC for 24 h under nitrogen atmosphere. After being cooled to room temperature, the mixture was extracted with CH_2Cl_2 and dried over Na_2SO_4. After the solvent was removed, the crude product was purified by column chromatography on silica gel to yield a yellow solid (1.74 g, yield 81%). ^{1}H NMR (500 MHz, $CDCl_3$) δ 8.86 (d, J = 8.1 Hz, 1H), 7.96 (d, J = 8.2 Hz, 1H), 7.79 – 7.65 (m, 12H), 7.65 – 7.61 (m, 2H), 7.61 – 7.50 (m, 6H), 7.46 – 7.40 (m, 2H), 7.37 (d, J = 8.8 Hz, 1H), 7.33 – 7.26 (m, 4H), 7.21 – 7.11 (m, 6H), 7.08 – 7.01 (m, 2H). ^{13}C NMR (126 MHz, $CDCl_3$) δ150.06, 147.64, 147.33, 141.17, 140.02, 139.76, 138.99, 138.83, 136.96, 134.39, 133.41, 130.76, 130.02, 129.83, 129.30, 128.86, 128.42, 127.61, 127.51, 127.22, 127.02, 126.77, 124.88, 124.50, 123.82, 123.01, 122.28. MS (MALDI-TOF, m/z): calcd for $C_{53}H_{37}N_3$, 715.30; found, 715.2834.

NI-2-DPhTPA (N,N-diphenyl-4'''-(1-phenyl-1*H*-naphtho[1,2-*d*]imidazol-2-yl)-[1,1':4',1'':4'',1'''-quaterphenyl]-4-amine*): NI-2-DPhTPA* was synthesized according to the procedure as described above for the synthesis of *NI-1-DPhTPA*, giving a yellow solid in 77% yield. ^{1}H NMR (500 MHz, $CDCl_3$) δ 8.43 (d, J = 8.8 Hz, 1H), 8.02 (dd, J = 21.1, 8.4 Hz, 2H), 7.86 (t, J = 8.6 Hz, 5H), 7.72 (m, J = 24.6, 14.2, 7.7 Hz, 11H), 7.59 – 7.47 (m, 3H), 7.41 – 7.24 (m, 8H), 7.15 (d, J = 7.1 Hz, 5H), 7.05 (d, J = 6.9 Hz, 3H). ^{13}C NMR (126 MHz, $CDCl_3$) δ 150.93, 147.64, 147.33, 141.12, 140.03, 139.76, 139.08, 138.65, 134.38, 131.68, 130.63, 130.29, 129.96, 129.73, 129.36, 129.12, 127.63, 127.36, 127.01, 126.71, 125.67, 124.71, 124.50, 124.32, 123.82, 123.01, 122.06, 120.18, 119.57. MS (MALDI-TOF, m/z): calcd for $C_{53}H_{37}N_3$, 715.30; found, 715.2834.

3-1*,* **3-2***,* **3-3***,* **3-4***,* **4-1***,* **4-2***,* **4-3***,* and **4-4** were synthesized according to the reported procedure.[6]

BIDPhTPA (N,N-diphenyl-4'''-(1-phenyl-1*H*-benzo[*d*]imidazol-2-yl)-[1,1':4',1'':4'',1'''-quaterphenyl]-4-amine*):* Toluene (60 mL), ethanol (20 mL), and 2 M aqueous Na_2CO_3

(15 mL) were added to a mixture of **3-4** (1.41 g, 3 mmol), 4'-bromo-N,N-diphenyl-[1,1'-biphenyl]-4-amine (1.24 g, 3.1 mmol), and $Pd(PPh_3)_4$ (100 mg, 3 mol%). The suspension was stirred at 90 ºC for 24 h under a nitrogen atmosphere. When cooled to room temperature, the mixture was extracted with CH_2Cl_2 and dried over Na_2SO_4. After the removal of solvent, the residue was purified by column chromatography on silica gel to afford a white solid (1.61 g, yield 81%). 1H NMR (500 MHz, $CDCl_3$) δ 7.95 (d, J = 8.0 Hz, 1H), 7.75 – 7.64 (m, 10H), 7.64 – 7.60 (m, 2H), 7.59 – 7.50 (m, 5H), 7.38 (ddd, J = 8.0, 5.3, 1.5 Hz, 3H), 7.33 – 7.26 (m, 6H), 7.18 – 7.12 (m, 6H), 7.10 – 7.02 (m, 2H). ^{13}C NMR (126 MHz, $CDCl_3$) δ 147.65, 147.33, 139.99, 139.75, 139.01, 138.85, 134.40, 130.29, 129.89, 129.72, 129.06, 128.26, 127.64, 127.37, 127.02, 126.72, 126.33, 125.78, 125.01, 124.50, 124.15, 123.83, 123.40, 122.82, 120.89. MS (MALDI-TOF-MS, m/z): calcd for $C_{49}H_{35}N_3$, 665.28; found, 666.2838.

PhIDPhTPA (N,N-diphenyl-4'''-(1-phenyl-1*H*-phenanthro[9,10-*d*]imidazol-2-yl)-[1,1':4',1'':4'',1'''-quaterphenyl]-4-amine*)*: *PhIDPhTPA* was synthesized according to the procedure as described above for the synthesis of *BIDPhTPA*, giving a white solid in 83% yield. ^1H NMR (500 MHz, $CDCl_3$) δ 8.78 (d, J = 8.3 Hz, 1H), 8.72 (d, J = 8.4 Hz, 1H), 7.77 (dd, J = 11.0, 4.0 Hz, 1H), 7.73 – 7.63 (m, 14H), 7.63 – 7.50 (m, 6H), 7.32 – 7.25 (m, 7H), 7.22 – 7.12 (m, 7H), 7.05 (t, J = 7.3 Hz, 2H). ^{13}C NMR (126 MHz, $CDCl_3$) δ 147.65, 147.33, 139.99, 139.75, 139.01, 138.85, 134.40, 130.29, 129.89, 129.72, 129.06, 128.26, 127.64, 127.37, 127.02, 126.72, 126.33, 125.78, 125.01, 124.50, 124.15, 123.83, 123.40, 122.82, 120.89. MS (MALDI-TOF, m/z): calcd for $C_{57}H_{39}N_3$, 765.31; found, 765.2965.

Device Fabrication and Characterization: hexaazatriphenylenehexacabonitrile (HATCN), di-[4-(N,N-di-p-tolyl-amino)-phenyl]cyclohexane (TAPC), N,N'-bis(naphthalen-1-yl)-N,N'-bis(phenyl)-benzidine (NPB), 4,4',4"-tris(carbazol-9-yl)triphenylamine (TCTA), 1,3,5-tri[(3-pyridyl)-phen-3-yl]benzene (TmPyPB), 2,2',2"-(1,3,5-benzinetriyl)-tris(1-phenyl-1-H-benzimidazole) (TPBi) were used as purchased from Luminescence Technology Co. without further purification. NI-1-DPhTPA, NI-2-DPhTPA, BIDPhTPA, and PhIDPhTPA were synthesized and sublimated by gradient temperature method before used. Glass substrates pre-coated with a 95-nm-thin layer of indium tin oxide (ITO) with a sheet resistance of 20 Ω per square were

thoroughly cleaned for 10 minutes in ultrasonic bath of acetone, isopropyl alcohol, detergent, deionized water, and isopropyl alcohol and then treated with O_2 plasma for 4 min in sequence. Organic layers were deposited onto the ITO-coated substrates by high-vacuum (< 5×10^{-4} Pa) thermal evaporation. Deposition rates were controlled by independent quartz crystal oscillators, which are 1~2 Å s^{-1} for organic materials, 0.1 Å s^{-1} for LiF, and 6 Å s^{-1} for Al, respectively. The emission area of the devices is 3 mm×3 mm as shaped by the overlapping area of the anode and cathode. EL spectrum was taken by an optical analyzer, Photo Research PR705. The luminance and current density versus driving voltage characteristics were recorded simultaneously with the measurement of CIE coordinates of these devices by combining the spectrometer CS200 with a Keithley model 2420 programmable voltage-current source meter. EQE values were calculated by assuming that the devices were Lambertian light sources. All measurements were carried out at room temperature under ambient conditions.

2. Summary of some representive reported performance of deep blue emitters.

Table S1. Summary of some representive reported performance of deep blue emitters.

Emitters	V_{on}[a] (V)	CE_{max} (cd A^{-1})	PE_{max} (lm W^{-1})	EQE_{max} (%)	V (V)	at 1000 cd m^{-2} CE (cd A^{-1})	at 1000 cd m^{-2} PE (lm W^{-1})	at 1000 cd m^{-2} EQE (%)	at 10000 cd m^{-2} V (V)	at 10000 cd m^{-2} CE (cd A^{-1})	at 10000 cd m^{-2} PE (lm W^{-1})	at 10000 cd m^{-2} EQE (%)	CIE (x,y)
fac-Ir(pmp)$_3$[1]	3	/[b]	/	10.1	8.7	/	/	9	-[c]	-	-	-	(0.16, 0.09)[d]
PtON7-dtb[2]	2.7	/	/	24.8	4.4	/	/	<8	-	-	-	-	(0.148, 0.079)[e]
DABNA-2[4]	4.2	21.1	15.1	20.2	-	-	-	-	-	-	-	-	(0.12, 0.13)[e]
3[5]	4.9	/	/	9.9	-	-	-	-	-	-	-		(0.15, 0.07)[e]
TSMA[7]	3.4	10.3	8.7	10.3	6.8	9.2	4.2	7	10.2	10.3	3.2	8	(0.14, 0.14)[f]
DPASP[8]	2.6	13	8.9	10.7	5.5	12	6.8	10.5	9	11	3.8	9.6	(0.14, 0.14)[f]
TBPMCN[9]	5	10.5	6.6	7.8	7.0	5.6	2.5	4.2	-	-	-		(0.16, 0.16)[e]
PMSO[11]	3.2	4.64	4	6.8	/	3.9	/	5.64	/	2.4	/	3.66	(0.152, 0.077)[e]
This Work Multilayer	2.6	6.94	7.79	6.43	3.5	6.7	6.01	6.21	5.2	5.67	3.43	5.26	(0.145, 0.120)[g]
This Work Simplified	2.6	4.95	4.96	5.12	3.9	4.86	3.96	5.02	6.1	4.04	2.08	4.22	(0.146, 0.104)[g]

[a] at the luminance of 1 cd m^{-2}; [b] the mark "/" indicates the data are not supplied; [c] the mark "–" means the device luminance is lower than the table title; [d] at the current density of 10 mA cm^{-2}; [e] not supplied; [f] at 8 V; [g] at a luminance of 10000 cd m^{-2}.

3. Density functional theory (DFT) calculation

Density functional theory (DFT) calculations were performed to obtain HOMO and LUMO energy levels by using the Gaussian suite of programs (Gaussian 09_B01).[10] The ground state structures were optimized by using B3LYP/6-31G(d, p) method in gas phase, and time-dependent density functional theory (TD-DFT) was employed to calculate the excited state energies on M062x/6-311G(d, p) level.

Table S2. Calculated HOMO and LUMO energy levels and excited state energies for BIDPhTPA, PhIDPhTPA, and NI-2-DPhTPA.

Compound	LUMO (eV)[a)]	HOMO (eV)[a)]	E_g^{cal} (eV)[a)]	E_S (eV)[b)]	E_T (eV)[b)]
NI-1-DPhTPA	-1.43	-4.92	3.49	3.86	3.01
NI-2-DPhTPA	-1.40	-4.92	3.52	3.87	3.10
BIDPhTPA	-1.43	-4.93	3.50	3.77	2.91
PhIDPhTPA	-1.40	-4.92	3.52	3.80	3.01

[a)] Obtained by density functional theory (DFT) calculations (B3LYP/6-31G(d,p), Gaussian 09_B01).

[b)] Obtained by time-dependent density functional theory (TD-DFT) calculations (M062X/6-311G(d,p), Gaussian 09_B01).

4. Calculated frontier orbitals of HOMOs and LUMOs of the emitters

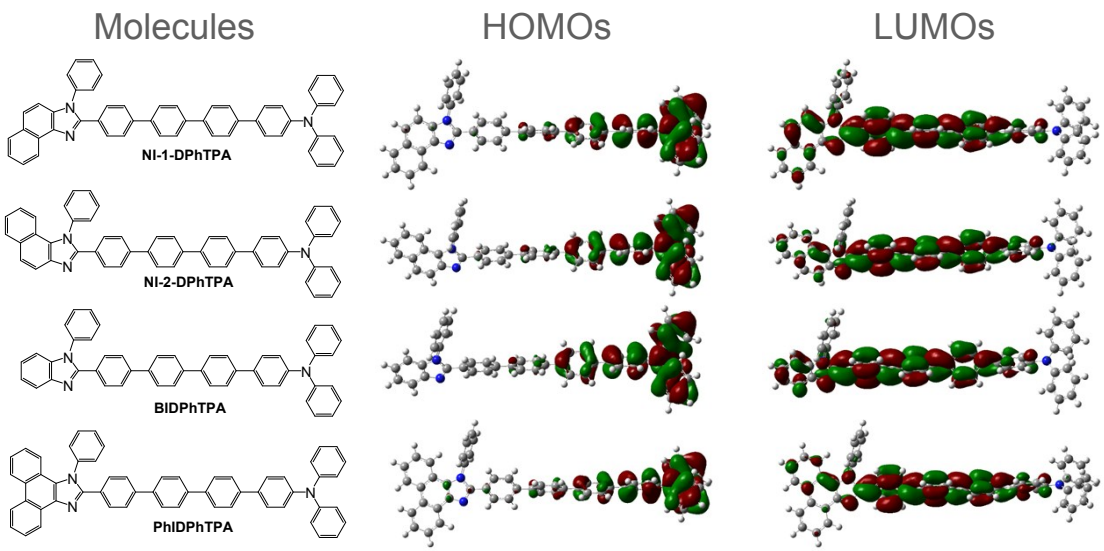

Figure S1. Calculated frontier orbitals of HOMOs and LUMOs of NI-1-DPhTPA, NI-2-DPhTPA, BIDPhTPA, and PhIDPhTPA (B3LYP/6-31G(d,p), Gaussian 09_B01).

5. Thermal analysis

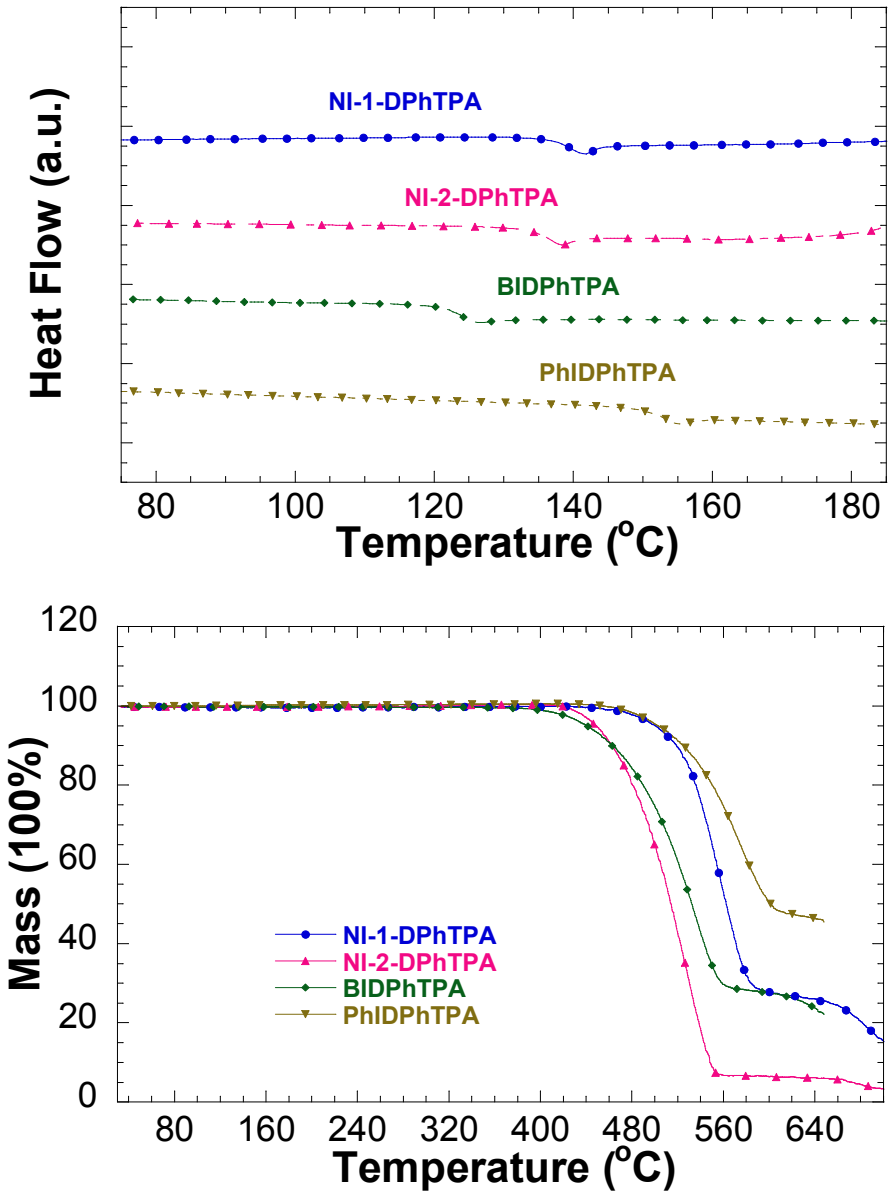

Figure S2. Differential scanning calorimetry (DSC, *top*), and thermogravimetric analysis (TGA, *bottom*) thermograms of NI-1DPhTPA, NI-2-DPhTPA, BIDPhTPA, and PhIDPhTPA.

6. Electrochemical cyclic voltammetry (CV)

The potential of the saturated calomel reference electrode was internally calibrated by using the ferrocene/ferrocenium redox couple (Fc/Fc^+), which has an absolute energy level of -4.8 eV. HOMO energy levels were calculated by the following equation.

$$HOMO = -(E_{ox} + 4.8\ eV) \quad (1)$$

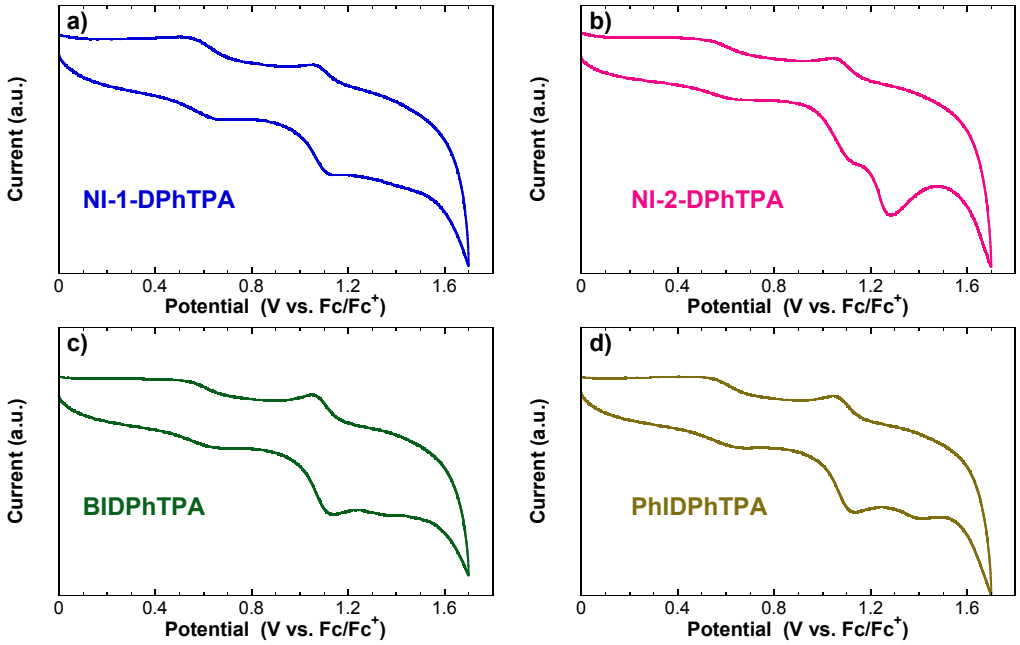

Figure S3. Cyclic voltammograms of the deep blue emitters NI-1-DPhTPA, NI-2-DPhTPA, BIDPhTPA, and PhIDPhTPA.

7. Photophysical properties in different solvents

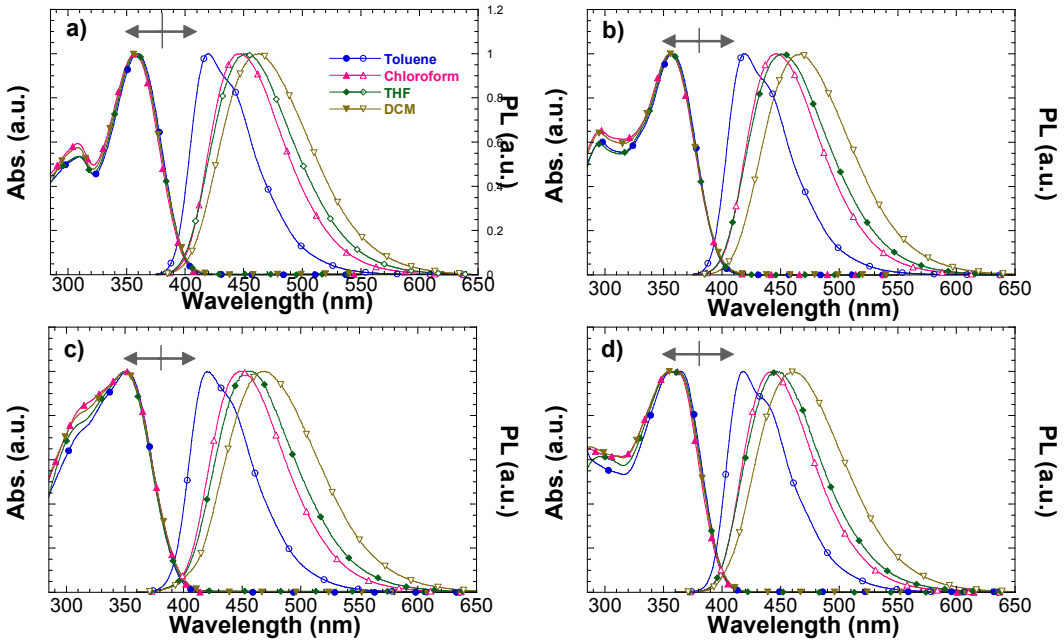

Figure S4. UV-vis absorption and photoluminescence spectra at room temperature of the blue emitters, a) NI-1-DPhTPA, b) NI-2-DPhTPA, c) BIDPhTPA, and d) PhIDPhTPA in toluene(●○), chloroform(▲△), tetrahydrofuran (◆◇), and dichloromethane (▼▽).

8. Physical properties and energy levels of the compounds

Table S3. Physical properties and energy levels of the compounds.

Compound	T_g/T_d[a] [°C]	λ_{abs}[b] [nm]	λ_{abs}[c] [nm]	λ_{em}[b] [nm]	λ_{em}[c] [nm]	PLQY[d]	E_g^{opt}[e] [eV]	HOMO/LUMO[f] [eV]
NI-1-DPhTPA	139.5/500.3	307, 357	305, 360	462	453	100 (53)	2.83	-5.18/-2.35
NI-2-DPhTPA	136.6/448.5	296, 355	300, 360	467	450	100 (81)	2.83	-5.18/-2.35
BIDPhTPA	119.6/440.4	-, 350	315, 354	467	453	100 (82)	2.89	-5.17/-2.28
PhIDPhTPA	148.5/502.6	287, 354	269, 364	461	448	100 (85)	2.89	-5.17/-2.28

a) Glass transition temperature (T_g) / decomposition temperature (T_d) (5% weight loss); b) UV-vis absorption bands and PL peaks measured in dichloromethane solutions at room temperature; c) UV-vis absorption and PL peaks in neat thin films; d) PL quantum yield (PLQY) of the emitters disolved in DCM at room temperature. The values in parentheses are PLQYs obtained from the neat solid thin films; e) Optical energy band gap (E_g^{opt}) estimated from the absorption edge in thin films; f) HOMO levels estimated from cyclic voltammetry and LUMO levels estimated from HOMOs and E_g^{opt}s.

9. Photophysical properties in thin film state

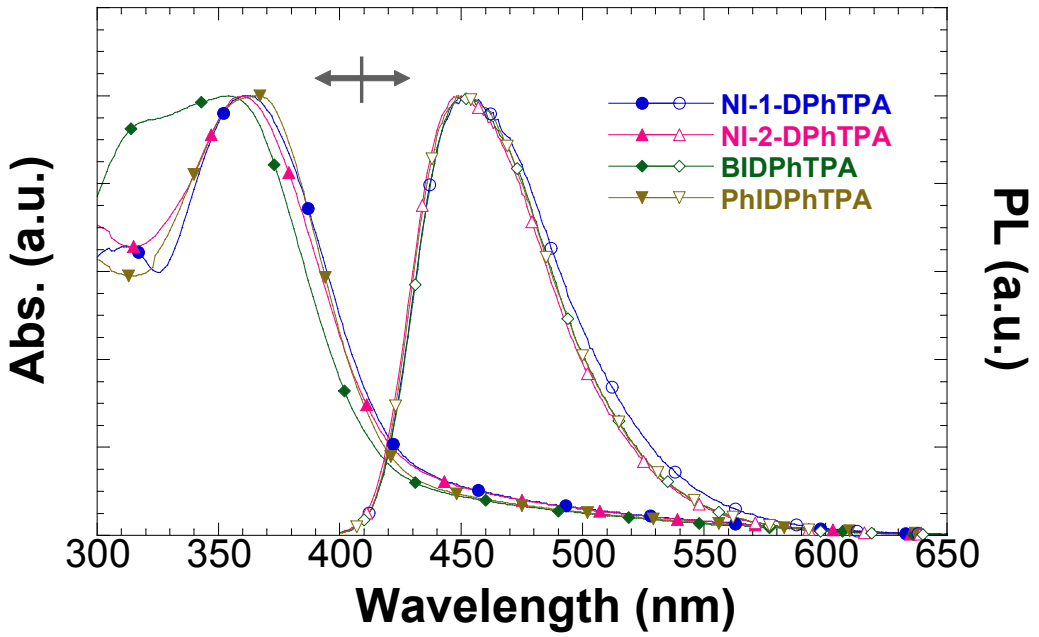

Figure S5. UV-vis absorption and PL spectra in thin solid film of NI-1-DPhTPA, NI-2-DPhTPA, BIDPhTPA, and PhIDPhTPA.

10. DFT optimized stable molecular configurations

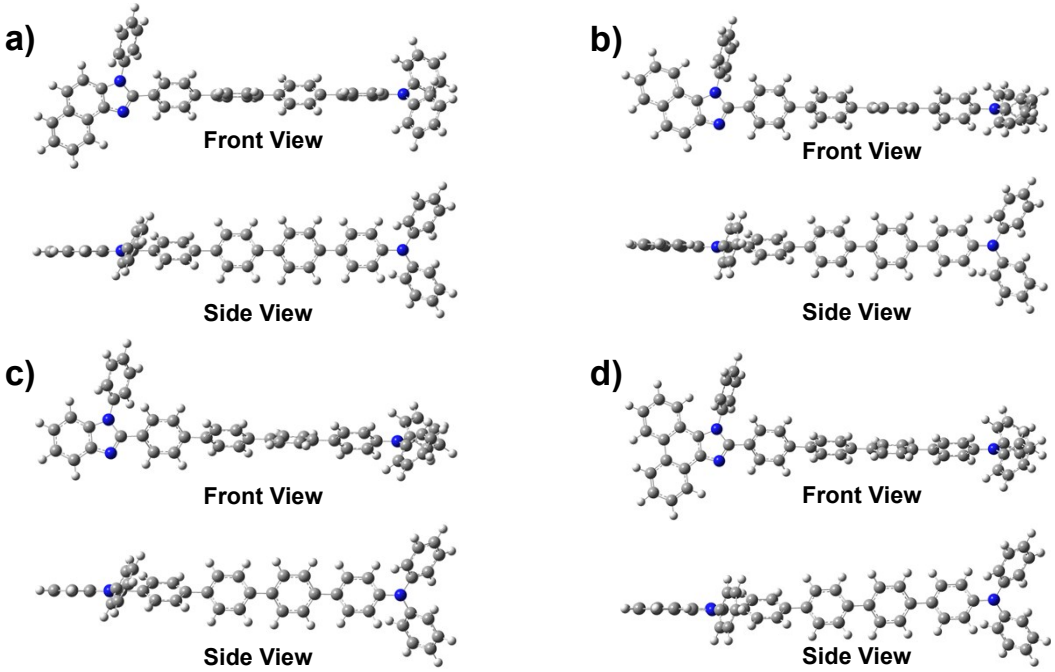

Figure S6. DFT optimized stable molecule configurations of the compounds, a) NI-1-DPhTPA, b) NI-2-DPhTPA, c) BIDPhTPA and d) PhIDPhTPA..

11. EL performance of multilayer OLED based on NI-1-DPhTPA.

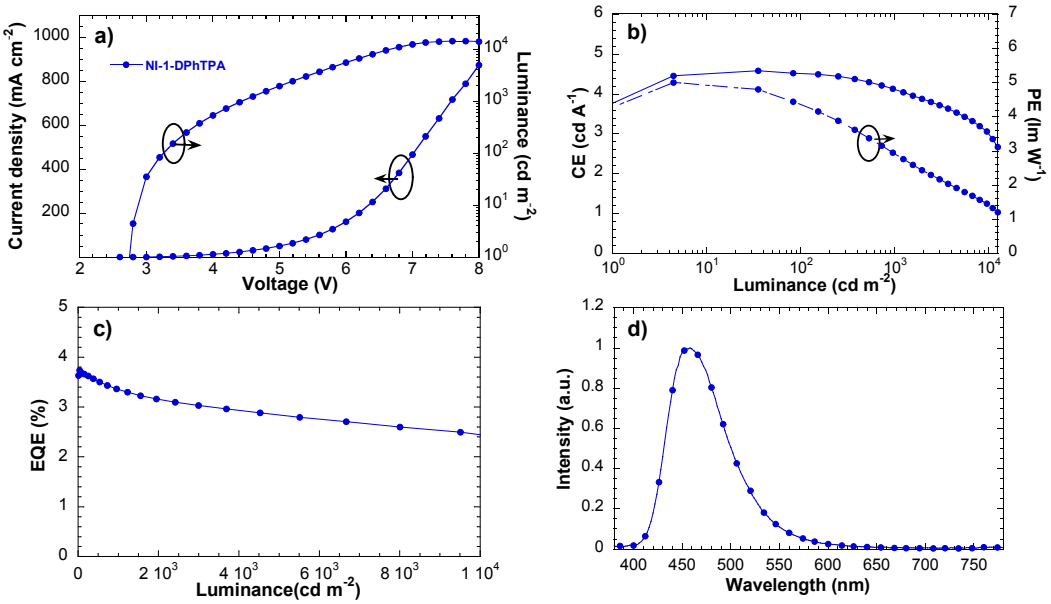

Figure S7. a) Current density and luminance versus driving voltage (J-V-L), b) current efficiency and power efficiency versus luminance (CE-L-PE), c) external quantum efficiency versus luminance (EQE-L) characteristics, and d) electroluminescence (EL) spectra at 10 mA cm^{-2} for the simple non-doped OLEDs in a structure of ITO/ NPB (40 nm)/ TCTA (5 nm)/ NI-1-DPhTPA (20 nm)/ TPBi (40 nm)/ LiF (1 nm)/ Al (marked as MS1).

12. Summary of the electroluminescent performance of MS1, SS1 and SS2.

Table S4. Summary of the electroluminescent performance of the tested multilayer non-doped device in a structure of ITO/ NPB (40 nm)/ TCTA (5 nm)/ NI-1-DPhTPA (20 nm)/ TPBi (40 nm)/ LiF (1 nm)/ Al (marked as MS1) and simplified device in a structure of ITO/ HATCN (5 nm)/ emitter (80 nm)/ LiF (1 nm)/ Al, emitter is NI-1-DPhTPA (marked as SS1), or PhIDPhTPA (marked as SS2).

Device	V_{on}[a]	CE_{max}	PE_{max}	EQE_{max}	at 1000 cd m^{-2}				
	(V)	(cd A^{-1})	(lm W^{-1})	(%)	V (V)	CE (cd A^{-1})	PE (lm W^{-1})	CIE (x,y)	EQE (%)
MS1	2.7	4.59	5.00	3.83	4.4	4.13	2.95	(0.149,0.139)	3.44
SS1	3.0	0.42	0.23	0.29	9.2	0.23	0.08	(0.162,0.159)	0.17
SS2	3.0	0.25	0.12	0.25	-	-	-	-	-

[a]at the luminance of 1 cd m^{-2}.

13. Transient PL decay

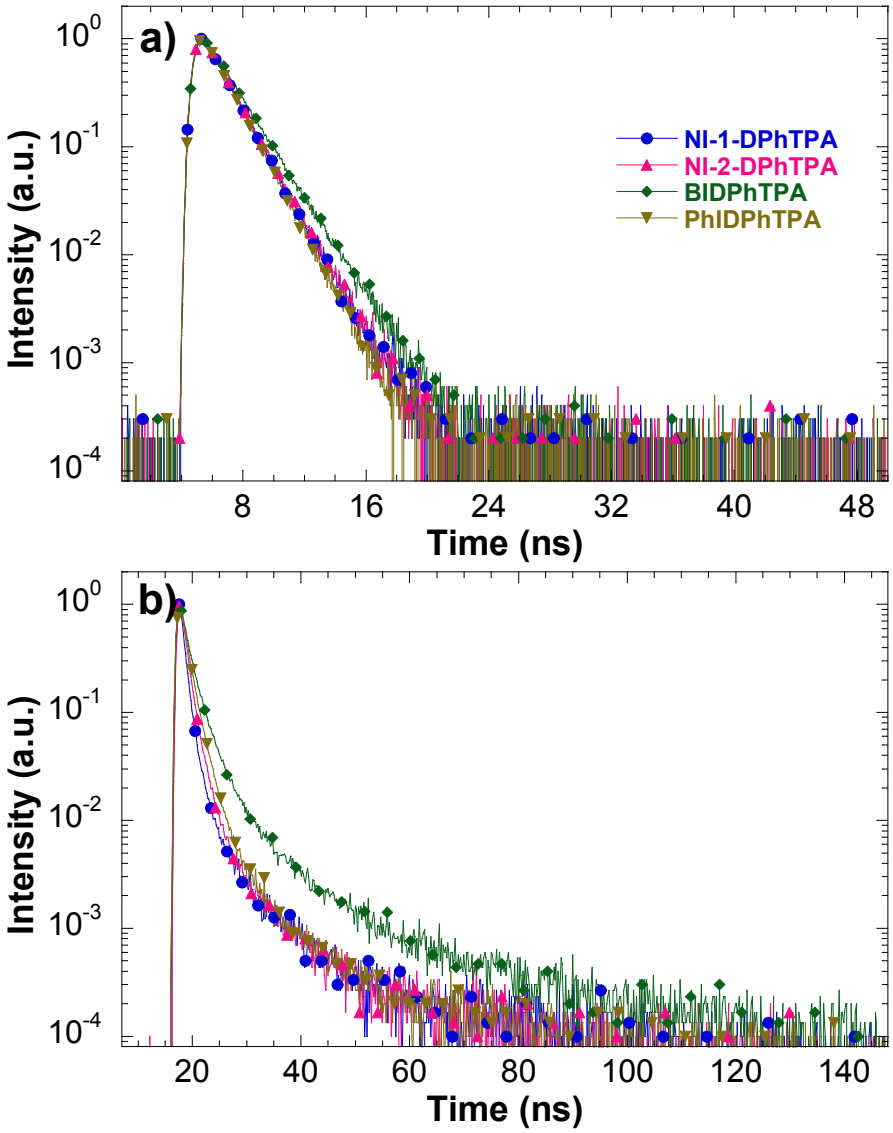

Figure S8. Transient PL decay curves of a) the solutions in DCM and b) neat solid films of NI-1-DPhTPA, NI-2-DPhTPA, BIDPhTPA, and PhIDPhTPA.

14. Dependence of the luminance of the simple non-doped blue OLEDs on the current density.

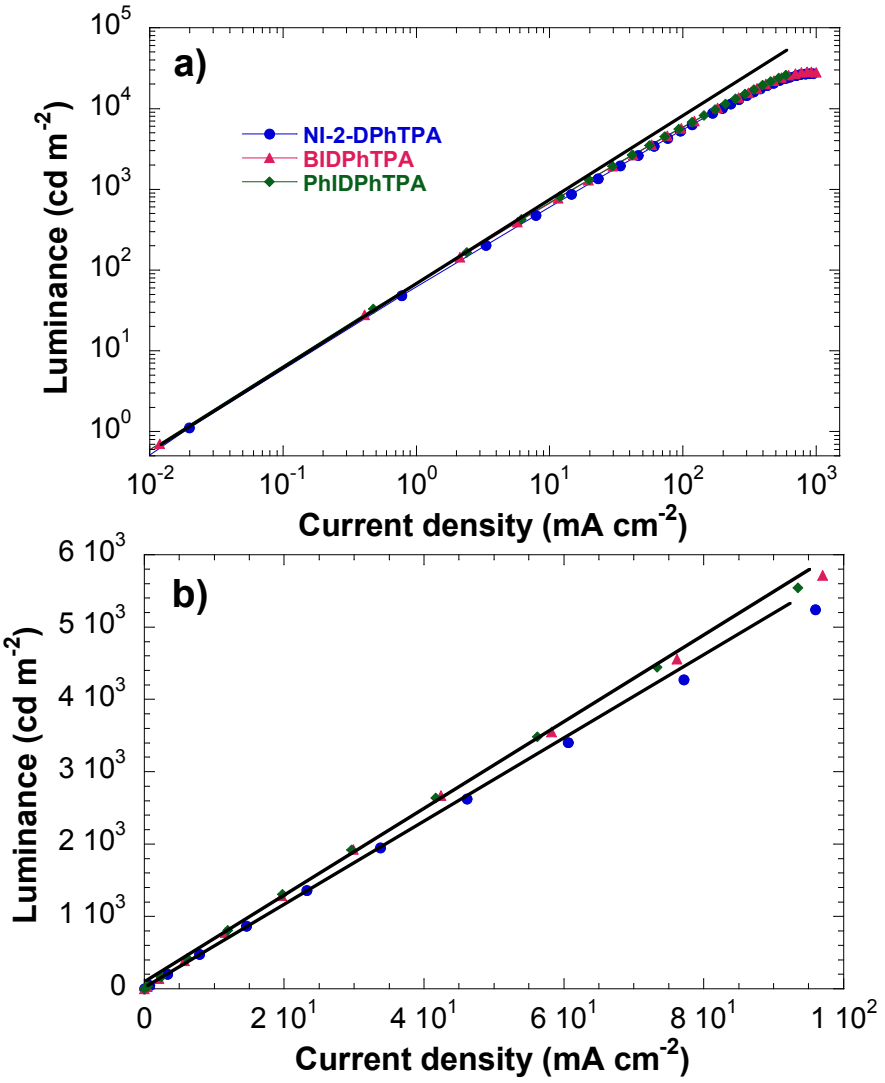

Figure S9. Dependence of the luminance of the non-doped blue OLEDs based on NI-2-DPhTPA (●), b) BIDPhTPA (▲), and c) PhIDPhTPA (◆) on the current density, a) High injection current, and b) Low injection current.

15. EL performance of simplified OLEDs based on NI-1-DPhTPA and PhIDPhTPA.

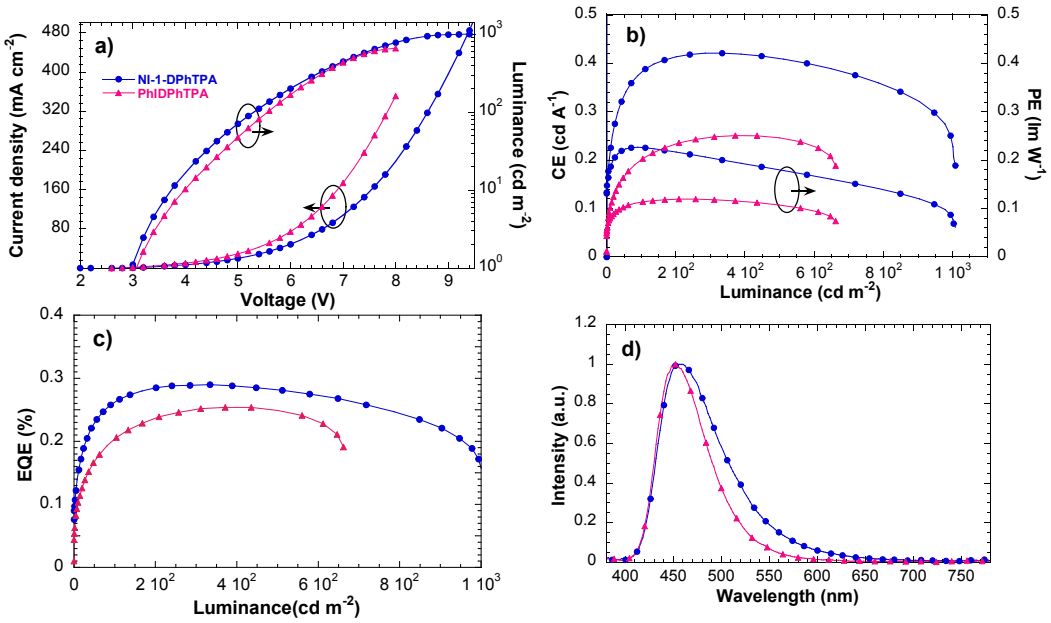

Figure S10. a) Current density and luminance versus driving voltage (J-V-L), b) current efficiency and power efficiency versus luminance (CE-L-PE), c) external quantum efficiency versus luminance (EQE-L) characteristics, and d) electroluminescence (EL) spectra at 10 mA cm^{-2} for the simplified non-doped OLEDs in a structure of ITO/ HATCN (5 nm)/ NI-1-DPhTPA (SS1, ●), or PhIDPhTPA (SS2, ▲) (80 nm)/ LiF (1 nm)/ Al.

16. EL spectra of multilayer non-doped and simplified OLEDs based on NI-2-DPhTPA and BIDPhTPA.

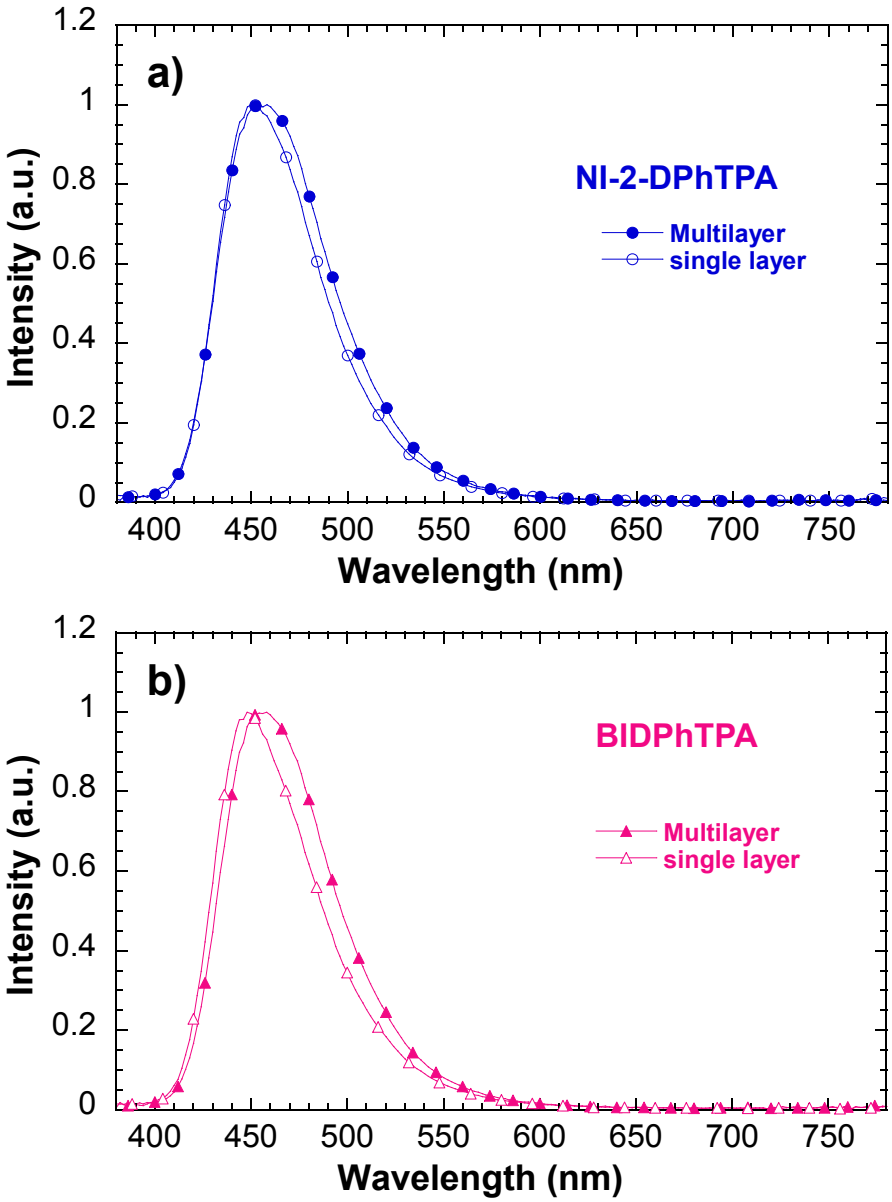

Figure S11. EL spectra of the multilayer non-doped and simplified OLEDs based on NI-2-DPhTPA and BIDPhTPA at 10 mA m^{-2}.

References:

1. J. Lee, H.-F. Chen, T. Batagoda, C. C., D. P. I., M. E. Thompson, S. R. Forrest, *Nat. Mater.,* 2016, **15**, 92.
2. T. Fleetham, G. Li, L. Wen, J. Li, *Adv. Mater.,* 2014, **26**, 7116.
3. M. Liu, X.-L. Li, D. C. Chen, Z. Xie, X. Cai, G. Xie, K. Liu, J. Tang, S.-J. Su, Y. Cao, *Adv. Funct. Mater.,* 2015, **25**, 5190.
4. T. Hatakeyama, K. Shiren, K. Nakajima, S. Nomura, S. Nakatsuka, K. Kinoshita, J. Ni, Y. Ono, T. Ikuta, *Adv. Mater.,* 2016, **28**, 2777.
5. Q. Zhang, J. Li, K. Shizu, S. Huang, S. Hirata, H. Miyazaki, C. Adachi, *J. Am. Chem. Soc.,* 2012, **134**, 14706.
6. S. Zheng, S. Diego, R. Bottger, *U.S. Pat. Appl. Publ.*, **US2011251401**, 13 Oct 2011.
7. P.-Y. Chou, H.-H. Chou, Y.-H. Chen, T.-H. Su, C.-Y. Liao, H.-W. Lin, W.-C. Lin, H.-Y. Yen, I.-C. Chen, C.-H. Cheng, *Chem. Commun.,* 2014, **50**, 6869.
8. Y.-H. Chen, C.-C. Lin, M.-J. Huang, K. Hung, Y.-C. Wu, W.-C. Lin, R.-W. Chen-Cheng, H.-W. Lin, C.-H. Cheng, *Chem. Sci.,* 2016, **7**, 4044.
9. S. Zhang, L. Yao, Q. Peng, W. Li, Y. Pan, R. Xiao, Y. Gao, C. Gu, Z. Wang, P. Lu, F. Li, S. Su, B. Yang, Y. Ma, *Adv. Funct. Mater.,* 2015, **25**, 1755.
10. M. J. Frisch, G. W. Trucks, H. B. Schlegel, G. E. Scuseria, M. A. Robb, J. R. Cheeseman, G. Scalmani, V. Barone, B. Mennucci, G. A. Petersson, H. Nakatsuji, M. Caricato, X. Li, H. P. Hratchian, A. F. Izmaylov, J. Bloino, G. Zheng, J. L. Sonnenberg, M. Hada, M. Ehara, K. Toyota, R. Fukuda, J. Hasegawa, M. Ishida, T. Nakajima, Y. Honda, O. Kitao, H. Nakai, T. Vreven, J. A. Montgomery Jr, J. E. Peralta, F. Ogliaro, M. J. Bearpark, J. Heyd, E. N. Brothers, K. N. Kudin, V. N. Staroverov, R. Kobayashi, J. Normand, K. Raghavachari, A. P. Rendell, J. C. Burant, S. S. Iyengar, J. Tomasi, M. Cossi, N. Rega, N. J. Millam, M. Klene, J. E. Knox, J. B. Cross, V. Bakken, C. Adamo, J. Jaramillo, R. Gomperts, R. E. Stratmann, O. Yazyev, A. J. Austin, R. Cammi, C. Pomelli, J. W. Ochterski, R. L. Martin, K. Morokuma, V. G. Zakrzewski, G. A. Voth, P. Salvador, J. J. Dannenberg, S. Dapprich, A. D. Daniels, Ö. Farkas, J. B. Foresman, J. V. Ortiz, J. Cioslowski, D. J. Fox, 2009, Gaussian.
11. X. Tang, Q. Bai, Q. Peng, Y. Gao, J. Li, Y. Liu, L. Yao, P. Lu, B. Yang, Y. Ma, *Chem. Mater.,* 2015, **27**, 7050.